Title
In situ measurement of velocity-stress sensitivity using crosswell continuous active-source seismic monitoring

Journal
Geophysics, 82(5)

ISSN
0016-8033

Authors
Marchesini, P
Ajo-Franklin, JB
Daley, TM

Publication Date
2017-09-01

DOI
10.1190/GEO2017-0106.1

GEOPHYSICS, VOL. 82, NO. 5 (SEPTEMBER-OCTOBER 2017); P. D319–D326, 6 FIGS., 1 TABLE.
10.1190/GEO2017-0106.1

In situ measurement of velocity-stress sensitivity using crosswell continuous active-source seismic monitoring

Pierpaolo Marchesini[1], Jonathan B. Ajo-Franklin[1], and Thomas M. Daley[1]

ABSTRACT

The ability to characterize time-varying reservoir properties, such as the state of stress, has fundamental implications in subsurface engineering, relevant to geologic sequestration of CO_2. Stress variation, here in the form of changes in pore fluid pressure, is one factor known to affect seismic velocity. Induced variations in velocity have been used in seismic studies to determine and monitor changes in the stress state. Previous studies conducted to determine velocity-stress sensitivity at reservoir conditions rely primarily on laboratory measurements of core samples or theoretical relationships. We have developed a novel field-scale experiment designed to study the in situ relationship between pore-fluid pressure and seismic velocity using a crosswell continuous active-source seismic monitoring (CASSM) system. At the Cranfield, Mississippi, CO_2 sequestration field site, we actively monitored seismic response for five days with a temporal resolution of 5 min; the target was a 26 m thick injection zone at approximately 3.2 km depth in a fluvial sandstone formation (lower Tuscaloosa Formation). The variation of pore fluid pressure was obtained during discrete events of fluid withdrawal from one of the two wells and monitored with downhole pressure sensors. The results indicate a correlation between decreasing CASSM time delay (i.e., velocity change for a raypath in the reservoir) and periods of reduced fluid pore pressure. The correlation is interpreted as the velocity-stress sensitivity measured in the reservoir. This observation is consistent with published laboratory studies documenting a velocity (V) increase with an effective stress increase. A traveltime change (dt) of 0.036 ms is measured as the consequence of a change in pressure of approximately 2.55 MPa (dP_e). For $T = 13$ ms total traveltime, the velocity-stress sensitivity is $dV/V/dP_e = dt/T/dP_e = 10.9 \times 10^{-4}/\text{MPa}$. The overall results suggest that CASSM measurements represent a valid technique for in situ determination of velocity-stress sensitivity in field-scale monitoring studies.

INTRODUCTION

Understanding time-varying reservoir properties has many applications, including production of oil and gas, production and storage of drinking water, and the geologic sequestration of CO_2. Seismic studies have long been a fundamental tool in determining reservoir properties and monitoring changes in those properties by way of induced variations in seismic wave propagation (Landrø and Stammeijer, 2004; Sayers, 2006; Duffaut et al., 2011). Although many interrelated attributes of seismic propagation are measured and studied (e.g., amplitude, phase, velocity, and attenuation), determining kinematic attributes of the propagating wave (e.g., seismic velocity) has perhaps the most widespread interest. Fluid pressure in porous reservoirs is one factor known to affect seismic velocity, and in situ measurements of the relationship between pressure (or stress) and velocity are rare, with most measurements using reflection amplitude variation to remotely estimate pore-pressure changes (Trani et al., 2011).

It is well-known that seismic velocity in porous rocks is a function of an effective stress state (e.g., Wyllie et al., 1958), generally increasing as a function of applied stress in the elastic regime. From a microstructural perspective, this effect is thought to be due to the closure of compliant cracks and the stiffening of grain contacts during the application of stress. Todd and Simmons (1972) summarize earlier measurements and show, with low-porosity granite and limestone cores, that the P-wave velocity is controlled by effective hydrostatic pressure P_e expressed as

Manuscript received by the Editor 16 February 2017; revised manuscript received 3 June 2017; published ahead of production 23 June 2017; published online 16 August 2017.
[1]Lawrence Berkeley National Laboratory, Energy Geosciences Division, Berkeley, California, USA. E-mail: pmarchesini@lbl.gov; jbajo-franklin@lbl.gov; tmdaley@lbl.gov.

$$P_e = P_c – \mathrm{nP_p} \quad (1)$$

rather than differential pressure, $P_e = P_c - P_p$, where P_c is the hydrostatic confining pressure, P_p is the pore pressure, n is the effective stress coefficient, following poroelasticity theory as developed by Biot (e.g., Biot and Willis, 1957). Berryman (1992) extends the theory of effective stress to various physical properties of rocks and shows each has a separate effective stress coefficient. Mavko and Vanorio (2010) give a recent overview of stress sensitivity, measurement, and theory, focused specifically on the impact of pore fluid and wave frequency on the stress dependence and the deviation of n from unity. All published measurements found of velocity as a function of varying stress at reservoir conditions have been made in the laboratory on core samples. For example, in a recent review, Angus et al. (2009) examine published stress versus velocity data for cores to constrain a stress-dependent microcrack rock-physics model.

Although these laboratory measurements are crucial to our understanding, there are limitations on obtaining unaltered core samples from deep formations (e.g., Holt et al., 2005), for example, in the case of shales, in which alteration during recovery and storage is common, particularly secondary microcrack formation due to gas exsolution. For large effective pressures, laboratory data can be fit to a linear trend (with an exponential relationship at lower pressures) as described by Shapiro (2003). This method was applied by Vernik and Hamman (2009), who limit the pressure range and avoided a low-porosity core from deep boreholes because of potential core damage. In addition to the problematic aspects of core integrity, most laboratory velocity-stress measurements are conducted at ultrasonic frequencies (approximately 10^5–10^6 Hz), well above those used to probe seismic properties in the field (approximately 10–10^3 Hz). The presence of velocity dispersion in systems with microcracks (e.g., Sams et al., 1997) provides a second source of uncertainty when using laboratory measurements to calibrate field measurements of stress.

With problems of deep core integrity affecting analysis, field-scale measurements at in situ conditions are needed to calibrate the velocity-stress relationship at high effective pressure. In addition, field-scale measurements can avoid some frequency-dependent effects related to high-frequency core measurements (Mavko and Vanorio, 2010) and directly incorporate the spatial averaging most relevant to field analysis, with the limitation being appropriate control of the measurement volume and in situ stress state. Field-scale measurements of stress sensitivity have generally focused on measurement of stress changes related to tectonics and earthquakes (Reasenberg and Aki, 1974; Furumoto et al., 2001; Niu et al., 2008) or monitoring of reservoir properties (often using analysis such as amplitude versus offset) (Landrø and Stammeijer, 2004; Sayers, 2006; Duffaut et al., 2011; Trani et al., 2011). In the case of monitoring reservoir properties, there are several factors that limit the certainty of remote measurements using surface seismic (e.g., Vasquez et al., 2010), with reservoir compaction often important for monitoring fluid withdrawal (Guilbot and Smith, 2002).

The crosswell continuous active-source seismic monitoring (CASSM) system has been applied to detect stress-induced seismic velocity changes for earthquake monitoring (Silver et al., 2007; Niu et al., 2008), to track changes in reservoir fluid saturation (Daley et al., 2010), and to monitor shallow hydraulic fractures (Ajo-Franklin et al., 2011). The CASSM method discussed in this paper is an in situ technique using the crosswell acquisition geometry to directly and continuously measure changes in traveltime within approximately 3.2 km deep reservoir unit along source-sensor raypaths. Because the source-sensor distance does not change, the fractional change in traveltime dt/T equals the fractional change in velocity dV/V. The goal of this study was to determine the relationship between pore-fluid pressure and seismic velocity in situ (i.e., the velocity-stress sensitivity) during a field hydraulic test. The repeatability and durability of CASSM make it the ideal acquisition technique for such a measurement. The relatively low amplitude of piezoelectric sources, compared with that of sources used in standard seismic surveys (mechanical sources), is overcome by stacking because the source position remains fixed for the whole duration of the experiment (Daley et al., 2007). The results suggest that coupling the CASSM system to standard hydrologic field tests may provide an avenue to estimate the stress sensitivity of velocity at field-relevant length scales early in long-term monitoring studies.

DATA ACQUISITION

Cranfield DAS site

The CASSM deployment at Cranfield, located near Natchez, Mississippi, was part of a detailed area study (DAS) site in a CO_2 sequestration test performed by the southeast regional carbon sequestration partnership (SECARB). The DAS site includes three boreholes, an injection well (31 F-1), and two monitoring wells (31 F-2 and 31 F-3) configured in a linear array (Figure 1). The project team selected the DAS site to examine multiphase fluid flow (supercritical CO_2/brine) and pressure effects at the interwell scale in a brine reservoir. As of 2012, the sequestration project has stored more than 3 million metric tons of CO_2. A description of the sequestration test is given by Hovorka et al. (2011). In addition, Ajo-Franklin et al. (2013) demonstrate the application of time-lapse crosswell seismic tomography to estimate the distribution and saturation of supercritical CO_2.

The approximately 26 m thick injection zone, in the lower Tuscaloosa Formation, is a fluvial sandstone with high vertical and lateral heterogeneity located in an anticlinal four-way closure at a depth of approximately 3.2 km. The Tuscaloosa Formation (D/E layers, Hovorka et al.,

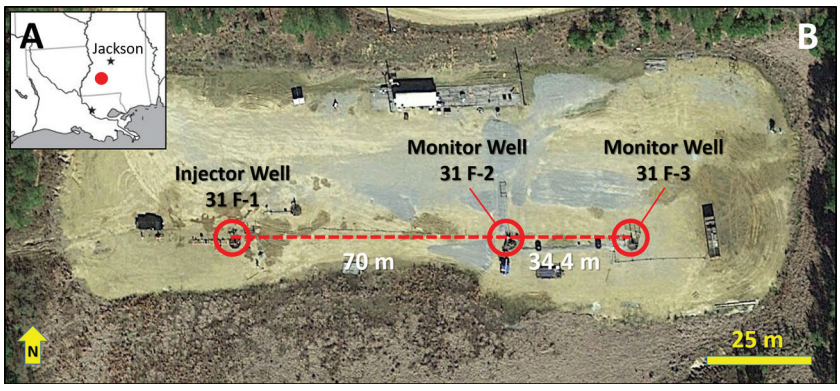

Figure 1. The Cranfield DAS site (red dot in insert A) located near Natchez, Mississippi, has three boreholes shown on the surface photo (insert B) with red circles (modified from Ajo-Franklin et al., 2013).

2011) is an oil-producing up-dip of the DAS site. The reservoir is composed of stacked and incised channel fills and is highly heterogeneous, with flow unit average porosities of 25% and permeability averaging 50 mD (millidarcy) and reaching up to 1 D (darcy). The confining stress (P_c) at the DAS site is approximately 65 MPa (Mavko et al., 2015) with preinjection pore pressure (P_p) of approximately 32 MPa (Delshad et al., 2013).

CASSM deployment and instruments

At the DAS site, a CO_2 injection well was coupled with two observation wells (Figure 1) along an azimuth toward the down-dip plume edge, sampling a portion of the evolving pressure field and supercritical CO_2 plume in approximately 26 m thick perforated, packer-isolated interval. The bottom hole well spacing (31 F-2 to 31 F-3) was initially measured as 41 m; however, recent analysis of crosswell seismic tomography indicates deviation measurement error, with a true spacing estimated at 34.4 m (Ajo-Franklin et al., 2013). Note that for estimating stress sensitivity from CASSM data, the distance is not a factor because we use traveltime changes (i.e., delay times *dt*) normalized by total traveltime *T*. The two monitoring wells had multiple instruments deployed on tubing including downhole pressure with real-time surface monitoring, an annular packer, U-tube fluid sampler, and the CASSM instruments (Hovorka et al., 2011). For the CASSM survey, two piezoelectric seismic sources (described in Daley et al., 2007) were deployed in well 31 F-2, concentric on the 2.875 in production tubing, and two hydrophone arrays were deployed in well 31 F-3, also on 2.875 in production tubing. The seismic sources have a center frequency of approximately 1.5 kHz, and use a single coaxial electrical connection to the surface power supply. The two sources were excited sequentially using a single high-voltage amplifier (approximately 2 kV) fed through a custom computer-controlled, high-voltage multiplexer. The drive signal for the amplifier, triggering of the recording system, and control of the switch were coordinated through a flexible MATLAB scheduling system and appropriate D/A cards (National Instruments). Figure 2 shows a schematic representation of this acquisition geometry with example raypaths. The locations of the sources and sensors were chosen following finite-difference waveform and eikonal ray-tracing numerical modeling, and with consideration of deployment logistical considerations, to give the best coverage of supercritical CO_2 movement in the reservoir along with "control" data above the reservoir. The actual source and sensor depths are given in Table 1.

The hydrophone arrays, fabricated by Z-Seis, consisted of two independently deployed systems (arrays 1 and 2), one above the reservoir section (sensors 1–5), and a second within the reservoir section (sensors 6–10), each using a seven-conductor electrical connection to the surface. All electrical lines, source and sensor, were tubing-encased conductors. Each hydrophone sensor is itself an array of eight individual hydrophones spanning 0.6 m length and wired together with a downhole amplifier, powered from surface electronics. The hydrophone arrays and the piezotube sources were pressure compensated to allow deployment at approximately 3.2 km

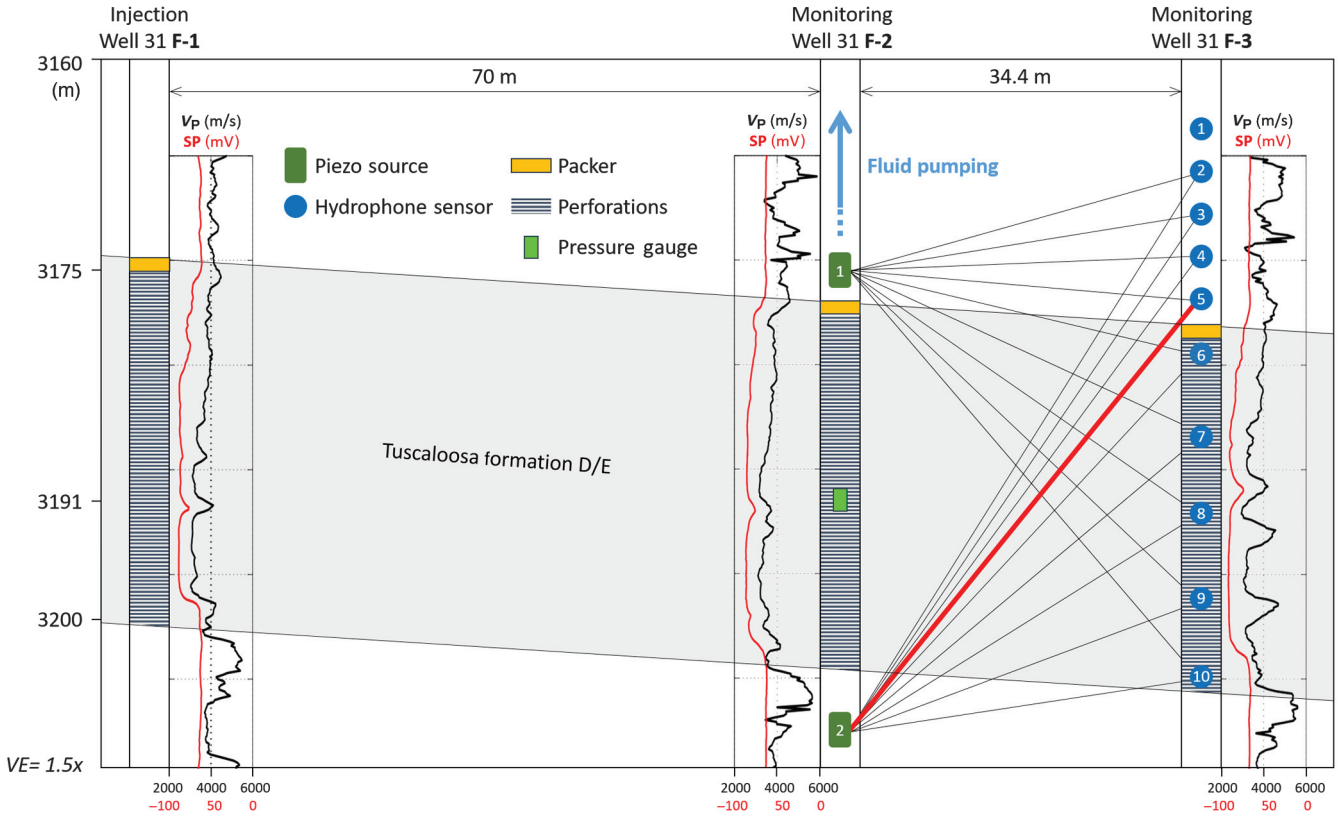

Figure 2. Schematic representation of CASSM data acquisition at the SECRAB Cranfield DAS. Raypaths from sources to hydrophone sensors are shown in black. Hydrophone sensor 1 failed during installation. Fluid was withdrawn from well 31 F-2 in three discrete events using a nitrogen lift procedure (Figure 4, pumping events 1–3). Data shown in Figures 3–5 are from the raypath shown in red (source 2 to sensor 5).

depth. The hydrophone arrays and CASSM sources were deployed in October 2009 and November 2009, respectively.

Initial testing of the CASSM sources found electrical crosstalk between the high-voltage source power pulse and the downhole pressure-temperature gauge, interrupting digital transmission. Because of the crosstalk, the source power was reduced to 800 V peak-to-peak, using a 1 ms width pulse. This is noted because the potential signal-to-noise level of the CASSM system is much higher than that shown here. With this modification, the CASSM system began recording on 13 November 2009, recording one record per source every 5 min, with each record being a stack of 25 source pulses (i.e., 25 stacks). The recording system was a Geometrics Geode seismograph, recording at 8000 samples per second (125 μs sample interval). Each record included all 10 hydrophone sensors plus a recording of the scaled source waveform and amplifier excitation signal. Figure 3 shows a sample recording, which is a temporal gather for one source-sensor pair (source 2 to sensor 5). Time delays are expected to be equal to zero because no pumping test was conducted during the time this temporal gather was recorded. The data acquisition continued with no interruptions until 18 November 2009, giving approximately five days of data during on/off fluid-pumping tests.

Table 1. The CASSM instruments depths.

Instrument	Location in well	Depth (from kB)
Source 1	31 F-2	3175 m
Pressure gauge	31 F-2	3191 m
Source 2	31 F-2	3208 m
Sensor 1 array 1	31 F-3	3165 m
Sensor 2 array 1	31 F-3	3168 m
Sensor 3 array 1	31 F-3	3171 m
Sensor 4 array 1	31 F-3	3174 m
Sensor 5 array 1	31 F-3	3177 m
Sensor 6 array 2	31 F-3	3186 m
Sensor 7 array 2	31 F-3	3191 m
Sensor 8 array 2	31 F-3	3195 m
Sensor 9 array 2	31 F-3	3200 m
Sensor 10 array 2	31 F-3	3204 m

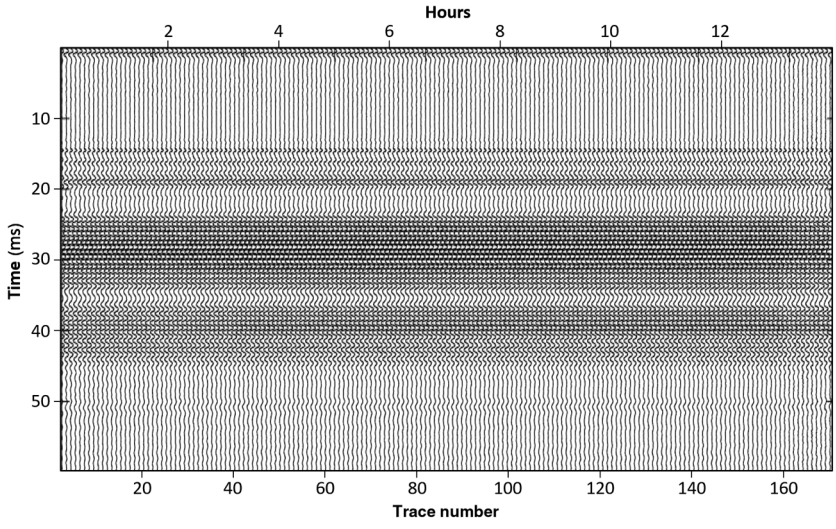

Figure 3. A temporal gather for source 2 to sensor 5 showing approximately 14 h of monitoring. One trace is recorded every 5 min. A band-pass filter (Ormsby filter 300–500–2000–4000 Hz) has been applied, and the data are normalized to the peak amplitude of the entire temporal gather.

Fluid-pumping tests

On 14 November 2009, a coil-tubing unit was used to produce fluid from well 31 F-2 (using the production tubing, through the CASSM sources). Following an initial pressure test of the well head and blow out preventer (an increase in annular well pressure above the packer), fluid was withdrawn from well 31 F-2 in three discrete events during 14–16 November 2009, using a nitrogen lift procedure (Figure 4, pumping events 1–3). A total of 876 barrels of fluid were produced from the well over three days. The downhole pressure was monitored and recorded with a quartz pressure/temperature gauge, fabricated by Kuster, installed on the production tubing of well 31 F-2, and placed within the perforated zone of the reservoir (Table 1). These pressure data are used as a measure of pore pressure (P_p) in the formation.

CASSM data processing

The CASSM processing was performed using Schlumberger VISTA and in-house Lawrence Berkeley National Laboratory's MATLAB seismic processing package, based on the downhole seismic imaging package described by Beaty et al. (2002). First, the field data were separated into source gathers. Then, we applied a band-pass filter (Ormsby filter 300–500–2000–4000 Hz) and sorted into source-sensor temporal gathers (Figure 3). Following the methodology presented by Silver et al. (2007), we subsampled the time series from 0.000125 (125 μs) to 0.000001 s (1 μs) in the frequency domain. This gather was windowed around the first arrival (e.g., 14–15.5 ms, in Figure 3), and each trace crosscorrelated with the first trace in the sequence with interpolation between samples, to obtain the delay time of the first arrival for each source-sensor pair at 5 min intervals. This delay time versus calendar time result is the base CASSM data to be compared with the varying pore pressure (Figure 4). A total of 18 CASSM data sets were collected, from nine sensors and two sources. Hydrophone sensor 1 failed during installation.

The fluid-pressure data were not modified from field recording except to remove nonphysical data "spikes" due to downhole electrical noise. All points at time $= t_i$, where pressure (P_i) was greater than 40 MPa (well outside the range of the test) or less than 0 MPa were discarded and replaced with the mean of the surrounding points $(P_{i-1} + P_{i+1})/2$.

RESULTS: CASSM DATA ANALYSIS

The analysis of reservoir changes focused on those source-sensor pairs, whose raypath crossed the entire reservoir interval (source 1 for sensors 7–10; source 2 for sensors 2–5). The CASSM data quality, as measured by random variation in time delay, was quite variable with standard deviation variation of more than two orders of magnitude between source-sensor pairs. The standard deviation was calculated over a 10 h time window, during which delay times are expected to be equal to zero (Figure 4, the time window centered around day 1). We did not use data whose standard deviation was greater than 100 μs. This limited the source-sensor pairs to 1–8, 1–9, 1–10, and 2–5, with the most consistent and interpretable response coming from source 2 to sensor 5 (Figure 2, red raypath). Our initial analysis consisted of a visual comparison of reservoir bottom-hole fluid pressure and time-delay changes for the source-sensor pair over the approximately five days of monitoring.

Figure 4 shows the pressure variation versus time-delay result for source 2 (just below the reservoir) and sensor 5 (just above the reservoir). The raw data curve, plotted as green points, shows a strong correlation with the CASSM time delay decreasing during periods of reduced pore pressure. This observation is consistent with velocity increasing when effective stress increases, as observed in laboratory studies. A drift in baseline traveltime delay is also observed, correlated with individual pumping phases; this delay change is suggestive of a secondary process changing formation properties independent of stress effects after each pumping test. One possible mechanism to explain this baseline change would be a gas exsolution process because the pore water is known to be saturated with respect to methane (CH_4) (Gao et al., 2012). The exsolved gas would reduce seismic velocity and dissolution could be a rate-limiting step in returning the system to a baseline velocity state. To remove this effect, we detrended the data by applying an adaptive median filter that corrects for individual dissolution trends happening after each exsolution event, and by subtracting the background trends to the original time series. The resulting data, plotted as blue points in Figure 4, effectively remove this background effect; an alternative detrending algorithm using a low-order spline fitting produced similar results. A final analysis was performed on the detrended data. Assuming no change in source-sensor distance (the tools are attached to production tubing and had been in place for weeks) the CASSM time-delay change (dt) can be directly interpreted as a velocity change in the reservoir (dV). The clearest anomalies are observed during the pumping between days two and three (referred to as pumping event 2) and between days three and four (referred to as pumping event 3). The same trend is observed in pumping event 1. Here, despite a substantial increase of pore pressure at the beginning of the pumping test (due to a wellhead pressure test), a subsequent decrease of pressure is matched by a decrease of traveltime delay during the duration of the pumping event.

After detrending, a linear fit can be constructed relating dt/T (the change in time normalized by total traveltime T) to the change in pressure as observed via the downhole gauge (P_p). Figure 5 shows the resulting data set and least-squares fits including the full data set (Figure 5a) and, alternatively, only the data within the vicinity of pumping event 2 (Figure 5b) and pumping event 3 (Figure 5c). Figure 5c shows the most consistent pumping response, i.e., the highest R^2. The analysis of the crossplotted data in Figure 5 shows that an even higher R^2 can be obtained by shifting the pore pressure data set 45 min later in time (Figure 5c′). A physical explanation for this observation relies on the delay in time needed by the reservoir to react to these rapid pressure changes. When the two data sets (time delays and pore pressure) are realigned with this shift, the calculation of the velocity/stress sensitivity becomes more accurate. Considering the 45 min shifted pore pressure data set and focusing on pumping event 3, a traveltime change (dt) of 0.036 ms is measured as the consequence of a change in effective pressure of approximately 2.55 MPa (dP_e). For $T = 13$ ms total traveltime, and average velocity V, the velocity-stress sensitivity of pumping event 3 is $dV/V/dP_e = dt/T/dP_e = 10.9 \times 10^{-4}$/MPa, assuming $n = 1$ and confining pressure is unchanged (Figure 5c′). Similarly, the resulting fits yield stress sensitivities $= 6.2 \times 10^{-4}$/MPa for the full data set (Figure 5a) $= 7.9 \times 10^{-4}$/MPa for pumping event 2 (Figure 5b), and $= 1.6 \times 10^{-4}$/MPa for pumping event 1 (not shown in figure). The rapid pore-pressure variation at the beginning of pumping event 1 is responsible for the resulting low velocity-stress sensitivity calculated for the pumping event and, more generally, for the full data set (Figure 5a). The stress sensitivity measurement is the fundamental result of this paper.

Uncertainty in the analysis is generated by the imperfect nature of the detrending process. The range 6.2×10^{-4} to 10.9×10^{-4}/MPa in pressure/delay crossplots, as shown in Figure 5, captures some of the variability in analysis strategies. To evaluate the feasibility of the 45 min pressure diffusion lag, we use the closed form for hydraulic pressure diffusion for a homogeneous porous media presented by Bear (1972). Assuming a porosity of 25%, a fluid viscosity of 2.4×10^{-4} Pa $*$ s (at in situ P-T conditions), an interwell distance of 30 m, a permeability of between 25 and 100 mD, and a total compressibility of between 10^{-8} and 10^{-9}/Pa, we can compute a range of likely hydraulic diffusion times analytically. The above parameter estimates are based on core and log measurements (porosity, permeability, and interwell distance) and available empirical models (brine viscosity); total compressibility is not well-constrained

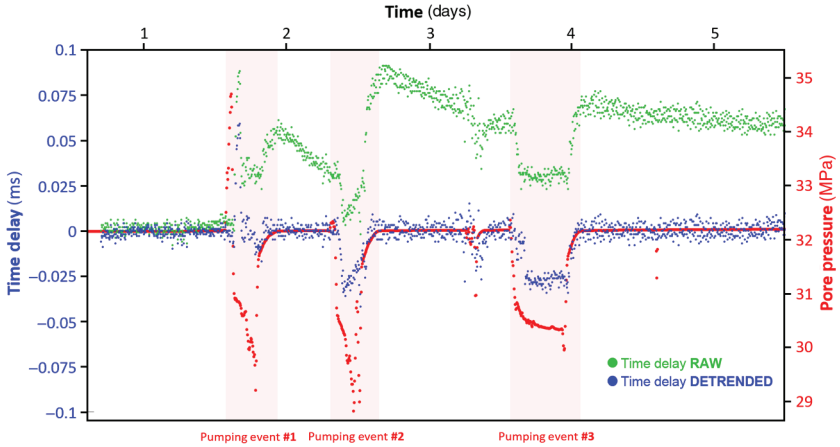

Figure 4. Temporal variation in crosswell time delay for the raypath from source 2 to sensor 5 (green = raw data; and blue = detrended data), with bottom-hole fluid pressure (red), over approximately five days of monitoring. The time between each successive data point is 5 min.

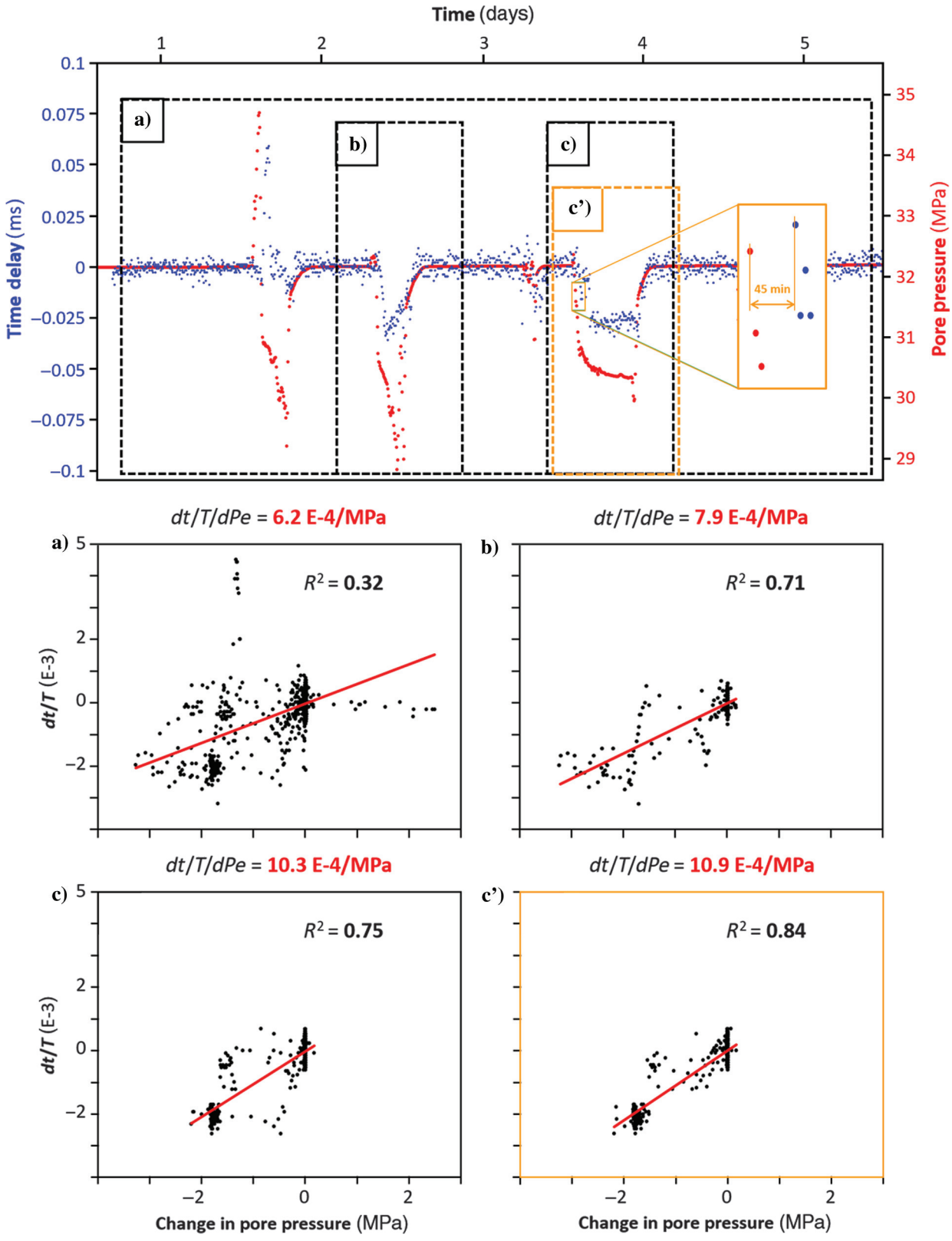

Figure 5. Detrended time-delay measurements for the raypath from source 2 to sensor 5 and pressure/delay crossplot analysis. The pressure dP_e versus dt/T regression results are shown for the full data set (a), and for the time portion including only the high-quality data proximal to the individual pumping events 2 (b), 3 (c), and 3 with the pore pressure data set shifted 45 min in time (c′).

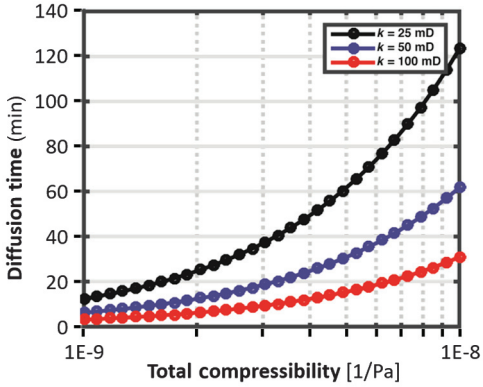

Figure 6. Estimates of interwell pressure diffusion time assuming homogeneous porous media and variable total compressibility values with low (25 mD), intermediate (50 mD), and high (100 mD) reservoir permeability scenarios.

hence we consider a range of values appropriate for intact rock. Figure 6 shows the resulting calculation for the previously mentioned range of compressibility values and mean permeabilities of 25, 50, and 100 mD. As can be seen, a 45 min diffusion time over this distance is feasible assuming that mean permeabilities are within the lower range (50 mD or lower) and total compressibilities are greater than 5×10^{-9}/Pa. Given the available site data, a more detailed hydrologic model could be constructed to evaluate the spatial distribution of pore-pressure perturbations generated by each pump test; however, such a calculation is outside the scope of this study.

It should be noted that this measured stress sensitivity is best considered a lower bound because we assume the entire reservoir thickness is changing in effective stress. More likely is that discrete high-permeability layers within the reservoir contain most of the pressure change, and therefore the stress sensitivity is higher in those layers. However, the average change over the entire reservoir is what is likely to be observed via changes in surface seismic response because of the longer elastic wavelengths used. From a rock-physics perspective, the relatively low value for stress sensitivity is also reflective of the high baseline effective stress state at Cranfield (Hovorka et al., 2009). Stress sensitivity is typically very high at low effective stress and decreases as the baseline effective stress increases, visible as a horizontal asymptote in velocity/stress plots. This phenomenon reflects the small number of compliant cracks, which remain open at high initial stress states (King, 1966).

CONCLUSION

A crosswell CASSM experiment was conducted to monitor injection of supercritical CO_2 in the lower Tuscaloosa Formation reservoir at a depth of approximately 3.2 km in the Cranfield DAS site. The instruments consisted of two tubing-deployed piezoelectric seismic sources and 10 tubing-deployed hydrophones. During a preinjection fluid-pump test, a change in crosswell traveltime between a fixed source and sensor pair was observed. The traveltime change shows a correlation with the pore pressure (P_p as measured by downhole pressure gauge in the perforated interval). This correlation is interpreted as the velocity-stress sensitivity, $dV/V/dP_e = dt/T/dP_e = 10.9 \times 10^{-4}$/MPa for the most consistent among three pumping event responses. Because of the uncertainty in the true pore-pressure distribution within the reservoir, we consider this measurement, the average over the approximately 26 m reservoir thickness, as a lower bound.

Stress sensitivity is an important parameter, used for seismic monitoring of reservoir pressure. Although core measurements can give accurate measurement of stress sensitivity, there are concerns over the upscaling to reservoir dimensions and the effects of unloading during core retrieval. Therefore, we believe this CASSM measurement offers a unique methodology for in situ determination of velocity stress sensitivity.

ACKNOWLEDGMENTS

We would like to thank S. Hovorka for her continuous support of CASSM technology; J. Hill and SECARB; B. Freifeld, P. Cook, and R. Solbau of LBNL; D. Freeman and Sandia Technologies; and Denbury Resources and the field staff at Cranfield. We thank V. Leung for initial data processing that was not used but encouraged further study. Use of VISTA software supported by GEDCO/WesternGeco and Schlumberger. This research was supported by the assistant secretary for Fossil Energy, Office of Natural Gas and Petroleum Technology, SECARB Program, and CSRP/GEO-SEQ Program, through the National Energy Technology Laboratory of the U.S. Department of Energy, under the U.S. DOE Contract No. DE-AC02-05CH1123. Additional funding for P. Marchesini was provided by Chevron. Secondary support for J. B. Ajo-Franklin was provided by U.S. Department of Energy, Office of Science, Office of Basic Energy Sciences, Chemical Sciences, Geosciences, and Biosciences Division under the U.S. DOE Contract No. DE-AC02-05CH11231.

REFERENCES

Ajo-Franklin, J. B., T. M. Daley, B. Butler-Veytia, J. Peterson, Y. Wu, B. Kelly, and S. Hubbard, 2011, Multi-level continuous active source seismic monitoring (ML-CASSM): Mapping shallow hydrofracture evolution at a TCE contaminated site: 81st Annual International Meeting, SEG, Expanded Abstracts, 3727–3731.

Ajo-Franklin, J. B., J. Peterson, J. Doetsch, and T. M. Daley, 2013, High-resolution characterization of a CO_2 plume using crosswell seismic tomography: Cranfield MS: International Journal of Greenhouse Gas Control, **18**, 497–509, doi: 10.1016/j.ijggc.2012.12.018.

Angus, D. A., J. P. Verdon, Q. J. Fisher, and J.-M. Kendall, 2009, Exploring trends in microcrack properties of sedimentary rocks: An audit of dry-core velocity-stress measurements: Geophysics, **74**, no. 5, E193–E203, doi: 10.1190/1.3183940.

Bear, J., 1972, Dynamics of fluids in porous media: Dover.

Beaty, K. S., G. Perron, I. Kay, and E. Adam, 2002, DSIsoft – A Matlab VSP data processing package: Computers and Geosciences, **28**, 501–511.

Berryman, J. G., 1992, Effective stress for transport properties of inhomogeneous porous rock: Journal of Geophysical Research, **97**, 17409–17424, doi: 10.1029/92JB01593.

Biot, M. A., and D. G. Willis, 1957, The elastic coefficients of the theory of consolidation: Journal of Applied Mechanics, **24**, 594–601.

Daley, T. M., R. D. Solbau, J. B. Ajo-Franklin, and S. M. Benson, 2007, Continuous active-source monitoring of CO_2 injection in a brine aquifer: Geophysics, **72**, no. 5, A57–A61, doi: 10.1190/1.2754716.

Daley, T. M., F. Niu, P. G. Silver, and E. L. Majer, 2010, Acquisition of crosswell seismic monitoring data: Handbook of geophysical exploration: Seismic Exploration, **40**, 165–176.

Delshad, M., X. Kong, R. Tavakoli, S. A. Hosseini, and M. F. Wheeler, 2013, Modeling and simulation of carbon sequestration at Cranfield incorporating new physical models: International Journal of Greenhouse Gas Control, **18**, 463–473.

Duffaut, K., P. Avseth, and M. Landrø, 2011, Stress and fluid sensitivity in two North Sea oil fields — Comparing rock physics models with seismic observations: The Leading Edge, **30**, 98–102, doi: 10.1190/1.3535438.

Furumoto, M., Y. Ichimori, N. Hayashi, and Y. Hiramatsu, 2001, Seismic wave velocity changes and stress build-up in the crust of the Kanto-Tokai region: Geophysical Research Letters, **28**, 3737–3740, doi: 10.1029/2001GL013172.

Gao, G., Z. Huang, J. Yuan, and C. Tong, 2012, The solution and exsolution characteristics of natural gas components in water at high temperature and pressure and their geological meaning: Petroleum Science, **9**, 25–30, doi: 10.1007/s12182-012-0178-9.

Guilbot, J., and B. Smith, 2002, 4-D constrained depth conversion for reservoir compaction estimation: Application to Ekofisk Field: The Leading Edge, **21**, 302–308, doi: 10.1190/1.1463782.

Holt, R. M., O.-M. Nes, and E. Fjaer, 2005, In-situ stress dependence of wave velocities in reservoir and overburden rocks: The Leading Edge, **24**, 1268–1274, doi: 10.1190/1.2149650.

Hovorka, S. D., J. W. Choi, T. A. Meckel, R. H. Treviño, H. Zeng, M. Kordi, F. P. Wang, and J. P. Nicot, 2009, Comparing carbon sequestration in an oil reservoir to sequestration in a brine formation — Field study: Energy Procedia: Proceedings of 9th International Conference on Greenhouse Gas Control Technologies, **1**, 2051–2056.

Hovorka, S. D., T. A. Meckel, R. H. Trevino, J. Lu, J. P. Nicot, J. W. Choi, D. Freeman, P. Cook, T. M. Daley, J. B. Ajo-Franklin, and B. M. Freifeld, 2011, Monitoring a large volume CO_2 injection: Year two results from SECARB project at Denbury's Cranfield, Mississippi, USA: Energy Procedia, **4**, 3478–3485, doi: 10.1016/j.egypro.2011.02.274.

King, M. S., 1966, Wave velocities in rocks as a function of changes in overburden pressure and pore fluid saturants: Geophysics, **31**, 50–73, doi: 10.1190/1.1439763.

Landrø, M., and J. Stammeijer, 2004, Quantitative estimation of compaction and velocity changes using 4D impedance and traveltime changes: Geophysics, **69**, 949–957, doi: 10.1190/1.1778238.

Mavko, G., and T. Vanorio, 2010, The influence of pore fluids and frequency on apparent effective stress behavior of seismic velocities: Geophysics, **75**, no. 1, N1–N7, doi: 10.1190/1.3277251.

Mavko, G., T. Vanorio, S. Benson, S. Vialle, A. Luttge, and R. Arvidson, 2015, Linking the chemical and physical effects of CO_2 injection to geophysical parameters: The Global Climate and Energy Project (GCEP), Stanford University, Final Technical Report, http://gcep.stanford.edu/pdfs/techreport2015/5.5.1%20Mavko%20(s&p).pdf.

Niu, F., P. G. Silver, T. M. Daley, X. Cheng, and E. L. Majer, 2008, Preseismic velocity changes observed from active source monitoring at the Parkfield SAFOD drill site: Nature, **454**, 204–208, doi: 10.1038/nature07111.

Reasenberg, P., and K. Aki, 1974, A precise, continuous measurement of seismic velocity for monitoring in situ stress: Journal of Geophysical Research, **79**, 399–406, doi: 10.1029/JB079i002p00399.

Sams, M. S., J. P. Neep, M. H. Worthington, and M. S. King, 1997, The measurement of velocity dispersion and frequency-dependent intrinsic attenuation in sedimentary rocks: Geophysics, **62**, 1456–1464, doi: 10.1190/1.1444249.

Sayers, C. M., 2006, Time-lapse seismic response to injection and depletion: 76th Annual International Meeting, SEG, Expanded Abstracts, 3195–3199.

Shapiro, S. A., 2003, Elastic piezosensitivity of porous and fractured rocks: Geophysics, **68**, 482–486, doi: 10.1190/1.1567215.

Silver, P. G., T. M. Daley, F. Niu, and E. L. Majer, 2007, Active source monitoring of crosswell seismic travel time for stress induced changes: Bulletin of Seismological Society of America, **97**, 281–293, doi: 10.1785/0120060120.

Todd, T., and G. Simmons, 1972, Effect of pore pressure on the velocity of compressional waves in low-porosity rocks: Journal of Geophysical Research, **77**, 3731–3743, doi: 10.1029/JB077i020p03731.

Toksoz, M. N., D. H. Johnston, and A. Timur, 1979, Attenuation of seismic waves in dry and saturated rocks: I. Laboratory measurements: Geophysics, **44**, 681–690, doi: 10.1190/1.1440969.

Trani, M., R. Arts, O. Leeuwenburgh, and J. Brouwer, 2011, Estimation of changes in saturation and pressure from 4D seismic AVO and time-shift analysis: Geophysics, **76**, no. 2, C1–C17, doi: 10.1190/1.3549756.

Vasquez, G., J. Justen, M. dos Santos, E. Vargas, Jr., and J.-L. Formento, 2010, Stress history of producing reservoirs and 4D seismic studies: Some often forgotten aspects: The Leading Edge, **29**, 814–818, doi: 10.1190/1.3462784.

Vernik, L., and J. Hamman, 2009, Stress sensitivity of sandstones and 4D applications: The Leading Edge, **28**, 90–93, doi: 10.1190/1.3064152.

Wyllie, M. R. J., A. R. Gregory, and G. H. F. Gardner, 1958, An experimental investigation of factors affecting elastic wave velocities in porous media: Geophysics, **23**, 459–493, doi: 10.1190/1.1438493.